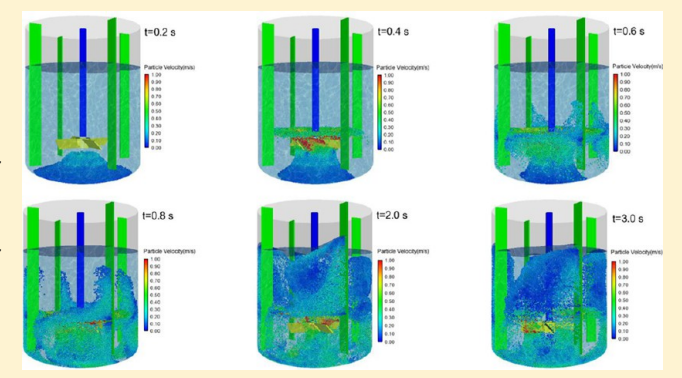


# Development of a DEM-VOF Model for the Turbulent Free-Surface Flows with Particles and Its Application to Stirred Mixing System

Liang Wu, Ming Gong, and Jingtao Wang\*

Supporting Information

**ABSTRACT:** The free-surface flows with particles are widely found in chemical engineering, and numerical modeling is a strong computing tool for in-depth understanding of the local and macrocharacteristics. In this study, a discrete element method-volume-of-fluid (DEM-VOF) model is extended to turbulent free-surface flows with particles, by means of Reynolds stress model. Also, we adopt a novel virtual dualgrid porosity model to calculate the fluid porosity. The simulated results of single particle sedimentation, the falling of sinking particles, and the floating of buoyant particles agree well to analytical and literatures, which validate the proposed DEM-VOF model. Furthermore, the DEM-VOF model developed in this paper is applied to the simulation of free



surface flow with particles in solid—liquid mixing system for the first time. It is found that elliptical-head vessel is preferred to a flat-bottomed vessel for solid-liquid mixing by comparing the simulation results of four different stirred tanks, which agrees well to the related content of the book Handbook of Industrial Mixing (Paul, E. L.; Atiemo-Obeng, V. A.; Kresta, S. M. Eds.; John Wiley & Sons, 2004).

#### 1. INTRODUCTION

The free-surface flows with particles are widely encountered in many fields relevant to granular media, such as energy, mineral, metallurgical, petroleum, environmental, pharmaceutics industries and materials, and geotechnical and chemical engineering. The engineering community has the pressing requirement for modeling the behavior of such complex three-phase flows at reasonable computational cost. For current computational capacities, it is unbearable to involve a direct numerical method to all the phenomena that arise in the multiphase flows. Therefore, the good multiphase model should provide reliable solutions with competitive cost.1-3

Dispersed particles are important in the physical of this problem and crucial in the major chemical and dynamical interactions with the flow system. Discrete element method (DEM) is a highly efficient and accurate model for capturing particle scale motion and interaction, and computational fluid dynamics (CFD)-DEM approaches have become very popular as they involve with the highly developed CFD techniques for the study of the complex fluid-particle flows. Zhu et al. have made complete reviews of CFD-DEM model.<sup>4,5</sup> It can be divided into two categories, the "resolved" and "unresolved", by the ratio of the particle sizes to the computational grid sizes. In the resolved CFD-DEM method, the solid particle phase is represented by a fictitious domain approach where the two phases share the one velocity and pressure field.<sup>6</sup> It can lead to extremely high computational cost, so the volume averaging method, unresolved CFD-DEM method, is widely accepted to address industrially significant problem. The unresolved CFD-DEM approach uses cell values or locally interpolated values for the evaluation of the fluid-particle interactions, which significantly reduces the computational burden.1 The interface-capturing volume-of-fluid (VOF) method is particularly interesting when used within the unresolved CFD-DEM couplings, as they allow solving the well-known single-phase equations within each single fluid phase.1

For modeling free-surface flows with particles, Gruber integrated the VOF model into CFD-DEM model where the VOF equations was artificially added with a source term. But this violates the conservation among the volume of three phases.<sup>7,8</sup> Jing proposed the volume-conservative model dealing with three phases.9 Chen has used DEM-VOF model to simulate the free-surface flows involving particles in rotating cylindrical tank. 10 Sun and Sakai 11 successfully combined the DEM model with the VOF model, and the volume conservation among three phases has been simulated by their model where the SDF representation and IB method are applied to model the complex geometries.<sup>11</sup> In order to reconstruct structures of the flow with a dimension similar to

November 22, 2017 Received: Revised: January 5, 2018 Accepted: January 15, 2018 Published: January 15, 2018



School of Chemical Engineering and Technology, Tianjin University, Tianjin 300072, People's Republic of China

<sup>\*</sup>School of Chemical Engineering, Northwest University, Xi'an 710069, Shaanxi People's Republic of China

the particle characteristic size, Pozzetti<sup>1</sup> proposed a novel dual-grid approach to resolve the bulk scale with information from the fluid fine scale, which extends the DEM–VOF method to the presence of multiscale complex interface dynamics. Currently, the DEM–VOF models developed by authors are in the verification stage<sup>1,9</sup> and the industrial applications of DEM–VOF model include the sloshing of liquid–solid particle mixtures,<sup>12</sup> three-phase dam break,<sup>11</sup> and wet ball milling in rotating cylindrical tank.<sup>10,11</sup>

However, there is no report about using the DEM-VOF model to simulate the free-surface flows with particles in solidliquid stirred tank, which is commonly used for suspending both types of solid particles, sinking and floating, in chemical and process industries. 13 Basically, a typical flow in solid-liquid stirred vessels with headspace involves fluid-particle interaction, particle-particle collision, and fluid-fluid interaction (evolving liquid-air interface). Most of the previous numerical are focus on the behavior of two-phase (respectively the particle phase and liquid phase), which all neglected the liquid free-surface. Tamburini 14,15 involved the two fluid model together with the sliding mesh model to research solid-liquid suspensions in stirred vessel, which includes baffles to prevent the formation of swirl on the surface of the liquid. Derksen simulated the turbulent dilutesuspensions flow by using an unresolved CFD-DEMh model, 16 and the resolved CFD-DEM approach was further developed by Derksen, to simulate the suspensions flows containing 3600 particles in a small-scale tank.<sup>17</sup> Shao involved the unresolved CFD-DEM coupled approach, based on FLUENT 6.3.26 and EDEM 2.2.1, to simulate the solid suspension behavior, in which the rotation and translation of millions of particles were taken into account.<sup>18</sup> Numerical simulations of the viscous solid-liquid flows in a flat-bottomed unbaffled tank were performed by Blais with the use of unresolved CFD-DEM model, which did not consider the liquid free-surface, 19,20 and he further extended the unresolved CFD-DEM to the turbulent flow.<sup>21</sup> But the above numerical studies all neglected the dynamic behavior of liquid free-surface, which usually appears in actual industrial vessels. The DEM-VOF model in this paper is extended to the turbulent free-surface flows with particles, especially for the solid-liquid mixing in stirred tanks. Because there is strong turbulence anisotropy, streamline curvature, and rotation that existed in unbaffled stirred tank or single baffle stirred tank, 13 our proposed DEM-VOF model considers the viscous force and Reynolds stress force of particles. In addition, we propose a novel dual-grid model for porosity calculations, which draws on the porous cube model made by Link,<sup>22</sup> Jing,<sup>9</sup> and dual-grid approach proposed by

The contents of this paper are as below: First, the equations of DEM model, the modified VOF model equations, the virtual dual-grid porosity model, and the coupling strategy are described in detail. Then, the validation tests of the model in the simulation of free-surface flows with particles is shown. The simulation of single particle sedimentation proves that the fluid-particle interaction crossing the water surface under different Reynolds numbers is correct. The simulation results about sinking particles falling into water and buoyant particles floating out of water show that the proposed model has the conservation of volume among three phases from both sides. Finally, the free-surface flows with particles in four different stirred tanks have been simulated and compared, which implies that an elliptical-head vessel is preferred to a flat-bottomed

vessel for solid—liquid mixing, which agrees well with prior empirical knowledge. As far as we know, the applications of the proposed DEM—VOF model to solid—liquid suspension of the agitator with headspace are for the first time.

#### 2. MODEL SPECIFICATION

A diagram of free-surface flows with particles is illustrated in Figure 1. In general, the two immiscible phases of fluid are

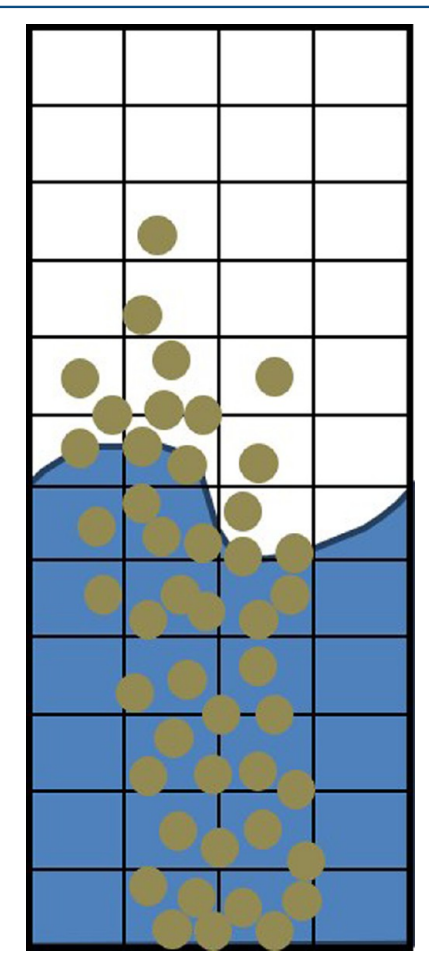


Figure 1. A system of free surface flows with particles.

separated by a distinct interface which is called the free surface. Particles could be located either in primary fluid or in the secondary fluid, and their motions are dominated by the interactions with the surrounding particles and fluid. The dynamic behaviors of the free-surface flows with particles are solved by coupling DEM model with VOF model. The equations of DEM model are presented in Section 2.1, and the modified VOF model equations are presented in Section 2.2. The particle-fluid interaction forces and calculation of mesh porosities are discussed separately in Section 2.3.1 and 2.3.2. The computing map of the entire system and the coupling map of the data exchanging are presented in Section 2.4.

**2.1. DEM Model.** The translation and rotation of all solid particles are accomplished by solving the Newton equation of motion<sup>4,5</sup>

$$m_i \frac{\mathrm{d}\nu_i}{\mathrm{d}t} = \sum_j \mathbf{F}_{c,ij} + \sum_k \mathbf{F}_{\mathrm{lr},ik} + \mathbf{F}_{\mathrm{pf},i} + \mathbf{F}_{\mathrm{g},i}$$
(1)

$$I_{i}\frac{\mathrm{d}\omega_{i}}{\mathrm{d}t} = \sum \left(\mathbf{M}_{t,ij} + \mathbf{M}_{r,ij}\right) \tag{2}$$

where  $m_i$ ,  $I_i$ ,  $v_i$ , and  $\omega_i$  represents the mass, the moment of inertia, the translational velocity, and angular velocity of particle i, respectively.  $\mathbf{F}_{c,ij}$ ,  $\mathbf{F}_{lr,ik}$ ,  $\mathbf{F}_{pf,i}$ , and  $\mathbf{F}_{g,i}$  indicate the contact force, the noncontact (long-range) forces, the interaction forces between particle-fluids, and a gravity force. The tangential and rolling friction moments are represent by  $\mathbf{M}_{t,ij}$  and  $\mathbf{M}_{r,ij}$ , respectively. The equations of the solid-fluid interaction forces rely upon what interaction forces are considered. This is explained in Section 2.3.1.

The key of the DEM model is the contact model between particles. The contact forces  $F_{c,ij}$  include the normal  $(F_{cn,ij})$  and tangential  $(\mathbf{F}_{\text{ct,}ij})^{4,5}$  component, which is described with the following equations

$$\mathbf{F}_{c,ij} = \mathbf{F}_{cn,ij} + \mathbf{F}_{ct,ij} \tag{3}$$

$$\mathbf{F}_{c,ij} = -k_{n,ij}\delta_{n,ij} - \gamma_{n,ij}\dot{\delta}_{n,ij} - k_{t,ij}\delta_{n,ij} - \gamma_{t,ij}\delta_{t,ij}$$
(4)

where  $k_{\text{n,ij}}$ ,  $k_{\text{t,ij}}$ ,  $\gamma_{\text{n,ij}}$ ,  $\gamma_{\text{t,ij}}$ ,  $\delta_{\text{n,ij}}$ , and  $\delta_{\text{t,ij}}$  indicate the normal stiffness coefficients, the tangential stiffness coefficients, the normal damping coefficients, the tangential damping coefficients, and the normal and tangential particle overlaps, respectively.  $\delta_{\mathrm{n},ij}$ and  $\dot{\delta}_{t,ii}$  represent their corresponding derivative terms in time.

In this work, the normal forces are calculated by the Tsuji model<sup>23</sup> and the tangential forces<sup>24,25</sup> are calculated by the Mindlin model. 26,27 These models are described by the equations in Table S1 (in the Supporting Information), where Y represent the material's Young's modulus, and  $\nu$  and  $e_r$  represent the Poisson ratio and coefficient of restitution.

2.2. VOF Model. In order to track the phase interface between two phases, the volume fraction of each fluid phase is added. In this study, there are only the primary phase and the secondary phase, and thus their volume fractions are denoted as  $\alpha_1$  and  $\alpha_2$ , respectively. Hence, there are three possible situations for the cell:  $\alpha_i = 0$ , indicating that the *i*th fluid is empty in the mesh cell;  $\alpha_i = 1$ , indicating that the *i*th fluid is full in the mesh cell;  $0 < \alpha_i < 1$ , meaning that the two fluids exist in the mesh cell. The dynamic behavior of the phase interface is the solution of the equation of continuity with the second fluid phase volume fraction<sup>28</sup>

$$\frac{\partial \alpha_2}{\partial t} + (\mathbf{u} \cdot \nabla)\alpha_2 = 0 \tag{5}$$

The volume fraction of primary fluid phase will be calculated by the equation below

$$\alpha_1 + \alpha_2 = 1 \tag{6}$$

The explicit and implicit time discretization can both be used to solve the equation of volume fraction. For transient VOF calculations, the explicit scheme should be used. In this work, the geometric reconstruction approach is used, which is the most accurate scheme in ANSYS FLUENT.<sup>28</sup>

The fluid density and viscosity are linearized by the present composition phases in each mesh cell

$$\rho = \alpha_1 \rho_1 + \alpha_2 \rho_2 \tag{7}$$

$$\mu = \alpha_1 \mu_1 + \alpha_2 \mu_2 \tag{8}$$

The well-known volume averaged governing equations<sup>29</sup> are used to describe the fluids phase motion. The continuity equation is

$$\frac{\partial \varepsilon_{\rm f}}{\partial t} + \nabla \cdot (\varepsilon_{\rm f} \mathbf{u}) = 0 \tag{9}$$

Because of highly swirling flows in unbaffled stirred tank or single-baffle stirred tank in which the important flow characteristics are influenced by the Reynolds stress anisotropy, the Reynolds stress model (RSM)<sup>30-32</sup> was adopted in this study. And the momentum equation is

$$\begin{split} & \rho_{\mathrm{f}} \Bigg( \frac{\partial (\varepsilon_{\mathrm{f}} \mathbf{u})}{\partial t} + \nabla \cdot (\varepsilon_{\mathrm{f}} \mathbf{u} \mathbf{u}) \Bigg) \\ & = \varepsilon_{\mathrm{f}} (-\nabla p + \nabla \cdot (\overline{\mathbf{\tau}} - \rho \overline{u_{i}' u_{i}'}) + \mathbf{f}_{\mathrm{s}} + \rho_{\mathrm{f}} \mathbf{g}) + \mathbf{f}_{\mathrm{pf}} \end{split} \tag{10}$$

where  $\varepsilon_{\rm f}$  represents the void fraction. The fluid density and velocity are represented by  $\rho_{\rm f}$  and  ${\bf u},$  respectively.  ${\bf f}_{\rm pf}$  represents the reacting force of the particle-fluid interaction term (1). The viscous stress tensor  $\tau$  is defined as

$$\overline{\tau} = \mu \left( (\nabla \mathbf{u}) + (\nabla \mathbf{u})^T - \frac{2}{3} (\nabla \cdot \mathbf{u}) \delta_k \right)$$
(11)

where  $\mu$  indicates the dynamic viscosity,  $\delta_k$  represents the identity tensor and  $\rho \overline{u'_i u'_i}$  represents the Reynolds stresses.

The CSF model are used to calculated the surface tension  $\mathbf{f}_s$ of free surfaces<sup>3</sup>

$$\mathbf{f}_{s} = \sigma \cdot \kappa \cdot \nabla \phi \tag{12}$$

where  $\sigma$  represents the surface force coefficient and  $\kappa$  represents the free-surface curvature, which is calculated by

$$\kappa = \frac{1}{|\mathbf{n}|} \left[ \left( \frac{\mathbf{n}}{|\mathbf{n}|} \cdot \nabla \right) |\mathbf{n}| \right] - (\nabla \cdot \mathbf{n})$$
(13)

where  $\mathbf{n} = \nabla \cdot \alpha_2$  is the normal vector.

 $\mathbf{f}_{pf}$  is a term of the momentum exchange between particle phase and fluid phase, and the expression of the momentum exchange term is

$$\mathbf{f}_{\mathrm{pf}} = \frac{1}{\Delta V} \sum_{i}^{n_{\mathrm{p}}} \mathbf{F}_{\mathrm{pf},i} - \mathbf{F}_{\nabla \mathrm{p},i} - \mathbf{F}_{\nabla \cdot \tau,i} - \mathbf{F}_{\nabla \cdot (\rho \overline{u_{i}' u_{j}'}),i} - \mathbf{F}_{\mathrm{s},i}$$

$$\tag{14}$$

where

$$\mathbf{F}_{\mathrm{pf},i} = \mathbf{F}_{\mathrm{d},i} + \mathbf{F}_{\mathrm{\nabla}_{\mathrm{p},i}} + \mathbf{F}_{\mathrm{\nabla}\cdot\tau,i} + \mathbf{F}_{\mathrm{\nabla}\cdot(\rho\overline{u_{i}u_{j}^{\prime}}),i} + \mathbf{F}_{\mathrm{s},i} + \mathbf{F}_{\mathrm{vm},i} + \mathbf{F}_{\mathrm{B},i} + \mathbf{F}_{\mathrm{Saff},i}$$

$$+ \mathbf{F}_{\mathrm{Mag},i}$$

$$(15)$$

and where  $\Delta V$  is the corresponding mesh cell volume and  $n_n$ indicates the particles number.  $F_{pf,i}$  represents the total of all interaction forces between particle-fluids: drag  $(F_{d,i})$ , pressure gradient  $(F_{\nabla p,i})$ , viscous stress force  $(F_{\nabla \cdot \tau,i})$ , Reynolds stress force  $(\mathbf{F}_{\nabla \cdot (\rho \overline{u_i'u_i'}),i})$ , capillary force  $(\mathbf{F}_{s,i})$ , virtual mass  $(\mathbf{F}_{vm,i})$ , Basset force  $(\mathbf{F}_{B,i})$ , Saffman lift  $(\mathbf{F}_{Saff,i})$  and Magnus lift  $(\mathbf{F}_{Mag,i})$ .

2.3. Particle-Fluids Interactions. 2.3.1. Interaction Forces. In DEM-VOF model, the expression of each interaction force contained in the term of fluid-particle interaction needs to be given. The drag force, pressure gradient force, viscous stress force, Reynolds stress force, capillary force, and lift forces, like Saffman lift force, Magnus lift force and fluid-induced torque, are all considered in this work. Table S2 (in the Supporting Information) lists the expression of these interaction forces.

2.3.2. Calculation of Mesh Porosities. The mesh porosity is important which could be used to calculate the drag force.

There are three kinds of models to calculate the porosity: the first model is so-called central model<sup>34,35</sup> in which the volumes of particles lied in one fluid mesh cell are summed; the second model is the divided model<sup>34,35</sup> which divides the particles into smaller equal portions; and the third model is named by the porous model, which can overtake numerical problems if the maximum particle size approaches the minimum mesh size. <sup>22,35–37</sup>

In this work, we develop a novel virtual dual-grid porosity model to calculate the mesh porosity, which is illustrated in Figure 2. It is derived from the recent study about a dual-grid

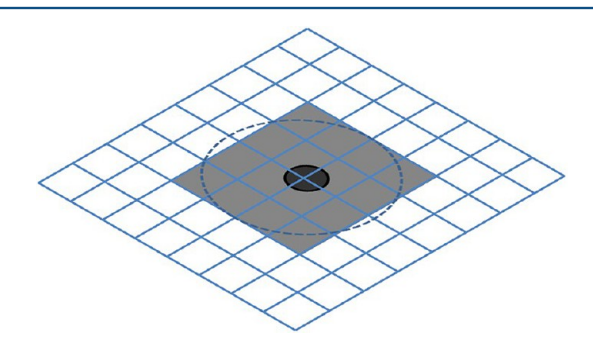


Figure 2. Schematic of the virtual dual-grid porosity model.

approach proposed to resolve the bulk scale with information from the fluid fine scale. The calculation of a considered particle to the mesh porosity is first calculated in a big coarse mesh cell that is virtual and is made up by a number of the actual mesh cells. The diameter of the big coarse mesh cell is several times the diameter of the particle. As illustrated in Figure 2, the big coarse mesh cell is the shaded region and made up by the shaded mesh cells. For particle j,  $d_{i,j}$  is used to represent the distance between the center of the shaded mesh cell i and that of particle j

$$\varphi_{j,i} = V_{p,j} / \sum_{d_{i,j} \le a \cdot R_j} V_{\text{cell},i}$$
(16)

where a is constant parameter and according to Jing<sup>9</sup> its recommend value is 4. The term in the right denominator of eq 13 represents the volume of the big coarse mesh cell for particle j. Herein  $\varphi_{i,j}$  is the rational average contribution of volume fraction particle j to the actual mesh cell i. In one fluid mesh cell i, its mesh porosity is the difference between the unit and the sum of the contributions of all particles to the mesh cell i

$$\varepsilon_{\mathbf{f},i} = 1 - \sum_{j} \phi_{j,i} \tag{17}$$

**2.4. Coupling Scheme.** The overall algorithm of DEM–VOF model is present in Figure 3 and is completed on commercial software ANSYS FLUENT and EDEM. At the beginning of the calculation, Fluent calls the user-defined initialization function which calls EDEM API to pass information on particle positions and calculates the mesh porosity and the fluid-particle interaction forces. In EDEM, the velocity and position of particles are updated through solving eqs 1 and 2 with source terms of particle—fluids interaction forces. According to the updated particle status, the calculations of the mesh porosity and the particle—fluids interaction forces are performed. Then, FLUENT performs the computing cycle by solving the eq 5 involving the volufraction, eqs 9 and 10 of the governing equations of the fluid, one by one, where the

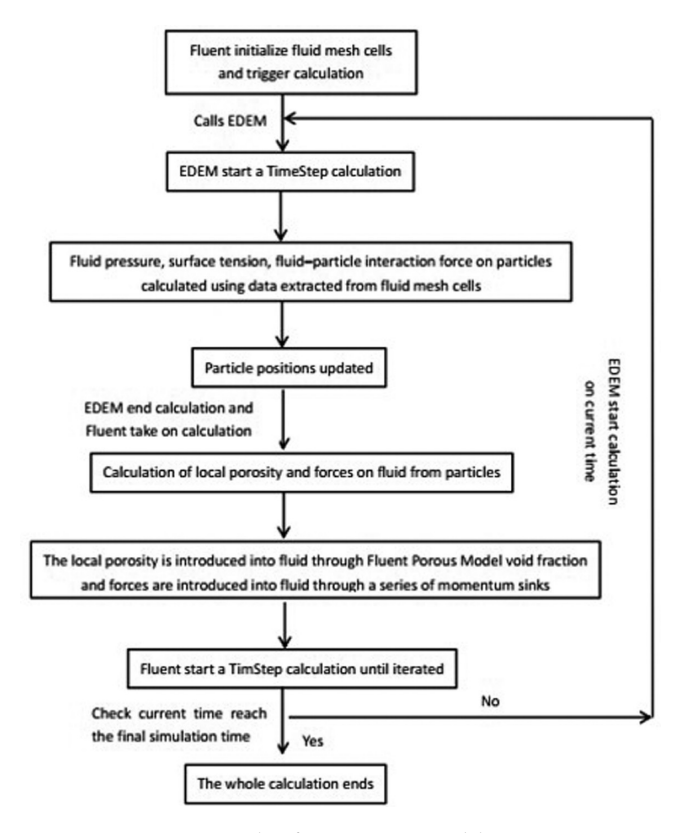


Figure 3. Computing cycle of DEM-VOF model.

transmission of mesh porosity and interaction forces information to the FLUENT side is through the void fraction of FLUENT Porous Model and a series of momentum source terms, respectively. Once the iteration is converged, the fluid cell status and the free surface are updated. Then, the computing cycle goes back to EDEM side, in which the particle—fluids interaction forces are calculated from the new fluid velocity field, and a new cycle starts.

## 3. VALIDATION OF DEM-VOF MODEL

In this section, DEM-VOF model proposed by us is validated. The correctness of DEM-VOF model is mainly determined by two characteristics: (a) the particle-fluids interaction forces and (b) the volume replacements among phases. Consequently, the validating tests are performed step-by-step: (1) single particle sedimentation and (2) water entry of particles.

In the first validating test, the single particle sedimentation is chosen to examine the correctness of the coupling scheme and the integration of particle—fluids interaction forces; in the second validating test, our results of water entry of particles are compared to those existing results of literatures to check whether the volume replacements among phases are correct or not.

**3.1. Single Particle Sedimentation.** For fluid-particle flows, single particle sedimentation is a basic but important problem, in which the single settling particle will eventually reach a steady velocity in a viscous fluid due to the balance between their gravity with the resistance of the fluid. To validate the accuracy of the DEM-VOF model, numerical analyses of a single particle falling through a water surface are performed. The domain dimensions are 4 mm × 4 mm × 8 mm, whose all wall boundary conditions are nonslip. The water surface is at half the height of the computational domain and

**Industrial & Engineering Chemistry Research** 

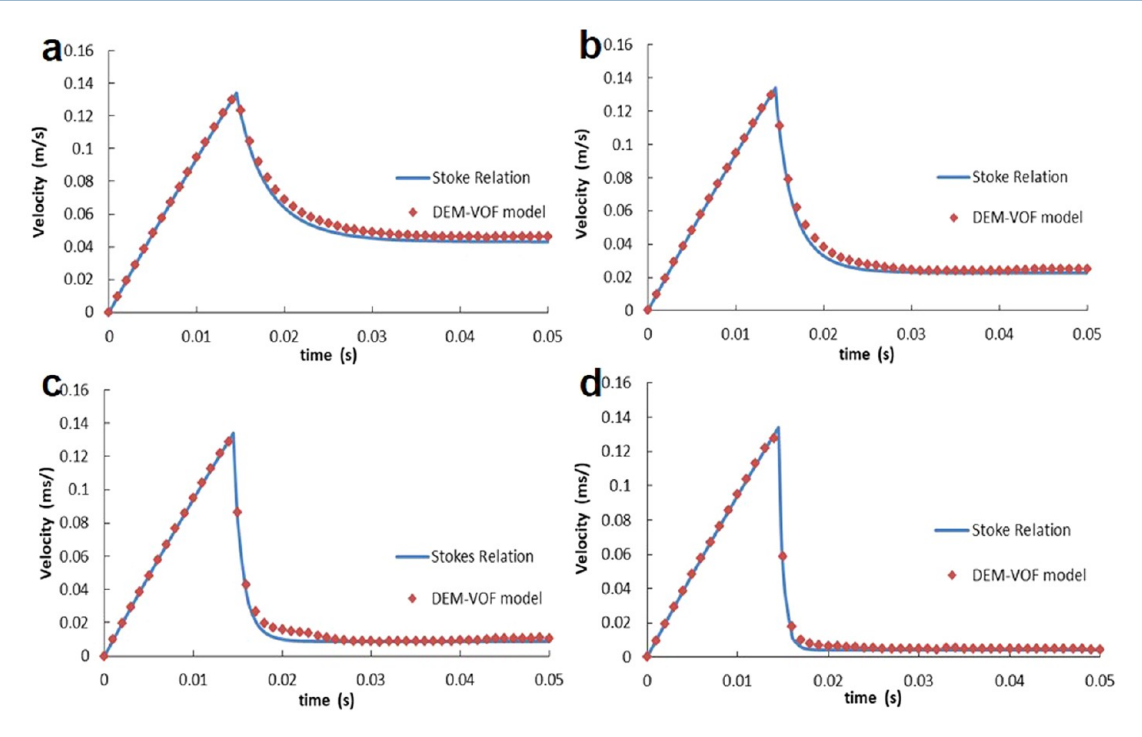


Figure 4. Velocity versus time for single particle falling from air into water at various water viscosities. (a)  $\mu_{\text{water}} = 0.00004 \text{ Pa·s}$ , Re = 107; (b)  $\mu_{\text{water}} = 0.0002 \text{ Pa·s}$ , Re = 11.34; (c)  $\mu_{\text{water}} = 0.0008 \text{ Pa·s}$ , Re = 1.09; (d)  $\mu_{\text{water}} = 0.002 \text{ Pa·s}$ , Re = 0.20.

the particle is placed 1 mm higher than the water surface. The entire computational domain uses a uniform grid of 0.25 mm, and the diameter of particles is 0.1 mm. The density of particles is 2500 kg/m³. The viscosity and density of the air phase are 1  $\times$  10 $^{-5}$  Pa·s and 1 kg/m³, respectively. The density of water phase is set to 1000 kg/m³ and its viscosity varies in different simulations in order to achieve different Re numbers.

Although the particle is considerably small, the fluid motions are still disturbed by the settling particle, and the disturbed fluid will affect the particle motion in turn. Thus, the actual calculating results differ from the theoretical results based on a static fluid domain. Similar to some other authors, <sup>34,38</sup> a low-Re flow regime is chosen for simplicity, where Stokes' law of drag are applied. Therefore, the motion of the single settling particle can be described by the equation below

$$\dot{\mathbf{v}} = -\frac{\rho_{\mathbf{p}} - \rho_{\mathbf{f}}}{\rho_{\mathbf{p}}} g - \frac{3\pi\mu_{\mathbf{f}} d_{\mathbf{p}}}{m_{\mathbf{p}}} \mathbf{v}$$
(18)

Four cases under various Re numbers are performed in this section. Water viscosities for different cases are  $4 \times 10^{-5}$ ,  $2 \times 10^{-4}$ ,  $8 \times 10^{-4}$ , and  $2 \times 10^{-3}$  Pa·s.

Curves of the settlement velocity with time variation and their analytical solutions are plotted in Figure 4 for four tests. Under these Reynolds numbers from  $1\times 10^{-1}$  to  $1\times 10^2$  orders of magnitude, the results of DEM–VOF model are in agreement with their approximate analytic solutions, which shows that the forces applied on the particle are correctly calculated and coupled. The particle sedimentation tests make it clear that the DEM–VOF model developed in the study can be used to calculate the settlement of single particle in two immiscible fluids at different Reynolds numbers.

**3.2. Water Interacts with Particle Swarm.** The falling of sinking particles and the floating of buoyant particles are interesting problems involving complicated free-surface motions and particle motions.<sup>11</sup> They can be used to validate the

correctness of DEM-VOF model, especially validate the volume replacement among three phases from both sides. As we know, the sinking particles will drive out the water in the vessel, and the height of water surface will be raised. Similarly, the buoyant particles will float out the water surface and the level of the water surface will be down. In this work, the simulation accuracy in volume conservation will checked by comparing the simulated change of water surface with theoretical solution. For water entry of sinking particles, the rising water surface height should be equal to the sum volume of all particles divided by the section area of the container, and the floating of buoyant particles is opposite.

In this section, the water entry of sinking particles is first simulated, and after all the particles sink to the bottom and the water surface is stable, then the density of water is set to 3 times of particle density in order to float particles up. In this simulation, the computational geometry dimensions are 0.05 m  $\times$  0.05 m  $\times$  0.20 m with the gravitational acceleration g = 9.81 $m/s^2$  in the z-direction. The geometry mesh size is 0.004 m. The boundary conditions of all side walls are set to no slip and the bottom of the tank whose top is open to the atmosphere. The entire system includes an air portion ( $\rho_g = 1.0 \text{ kg/m}^3 \text{ and}$  $\mu_{\rm g} = 10^{-5} \, {\rm Pa \cdot s}$ ) and a water portion ( $\rho_1 = 1000 \, {\rm kg/m^3}$  in falling simulation,  $\rho_1 = 7500 \text{ kg/m}^3$  in floating simulation, and  $\mu_1 =$ 10<sup>-3</sup> Pa·s). Their boundary, namely the water free surface, initially locates at z = 0.05 m. Totally 9600 particles aligned on a 20  $\times$  20  $\times$  25 lattice, placed above the water level. The diameter of particles  $(d_p)$  is 2.0 mm and their distance is 2.01 mm. The particle density is set to  $\rho_p = 2500 \text{ kg/m}^3$ , their Shear Modulus are 10<sup>7</sup> Pa, and Poisson's Ratio is 0.25. As for interaction parameters used by DEM, the coefficient of restitution between particles is 0.2, the static friction coefficient is 0.5 and the rolling friction coefficient is 0.01. The simulation conditions are similar to those of the literature. 11 Thus, the correctness of the calculation results can be explained by comparing with the literature results. The time step of DEM is  $2 \times 10^{-5}$  s and the time step of the continuum phase is  $10^{-4}$  s. The falling simulation runs up to t = 2.0 s after the particles all get settled and the water free surface restores calm. Then, the density of water is set to 3 times of particle density to simulate the floating of buoyant particles, which runs up to t = 3.5 s.

In the following figures, the particles are marked by three colors according to their initial height; the top portion is red, the middle is green, and the bottom is blue, which makes it easy to observe the topological change of particle swarm. A series of snapshots of particles falling into water is shown in Figure 5.

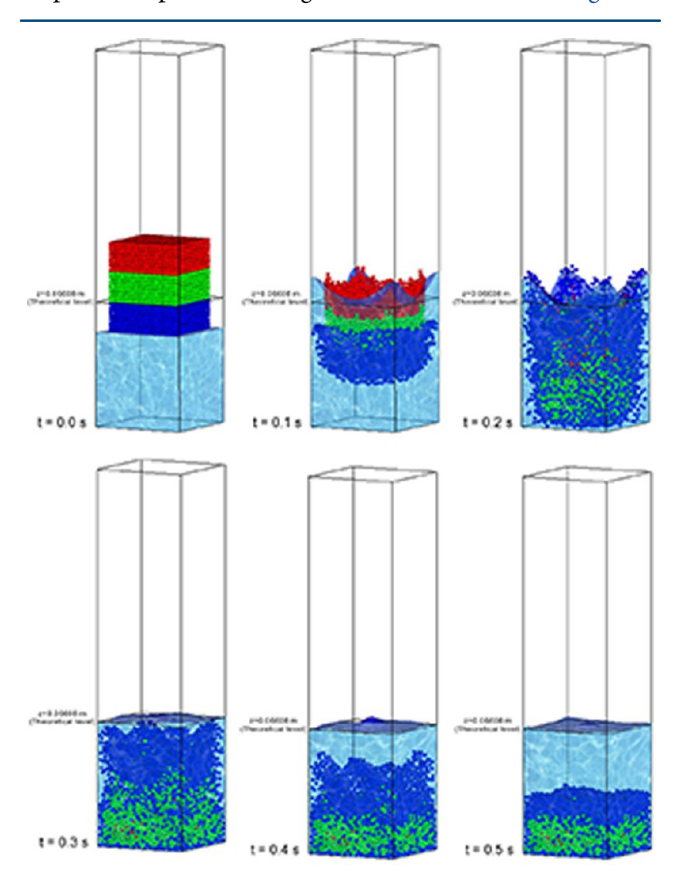


Figure 5. Snapshots of sinking particles falling into water.

Particles fall cross the surface of water under the action of gravity at about t = 0.1 s, which approaches the time of a free falling. Meanwhile, the bottom particles were first subjected to water resistance and move laterally. The water was also subjected to the action of particles, rising along the four corners. When all the particles were submerged below the water (t = 0.2 s), they began to sink, and the water surface became sloshing freely. Because the bottom particles were first subjected to water surface resistance, the part of the bottom particles flipped into the higher area, especially at the four corners. Then, the part of bottom particles was elevated by the rising water surface and this part of bottom particles was at the top when it is settling. Consequently, the red particles (initially at the top) were covered by two separated layers of the blue particles in the final settlements. This dynamic phenomenon is consistent with Sun and Sakai. 11 To further verify the accuracy of the proposed model, the water surface that went down in the case of particles floating out of water was simulated. A series of snapshots of particles floating out of water is presented in Figure 6. This was an amusing phenomenon that the floating speed of particles in the center part and four corners was slower

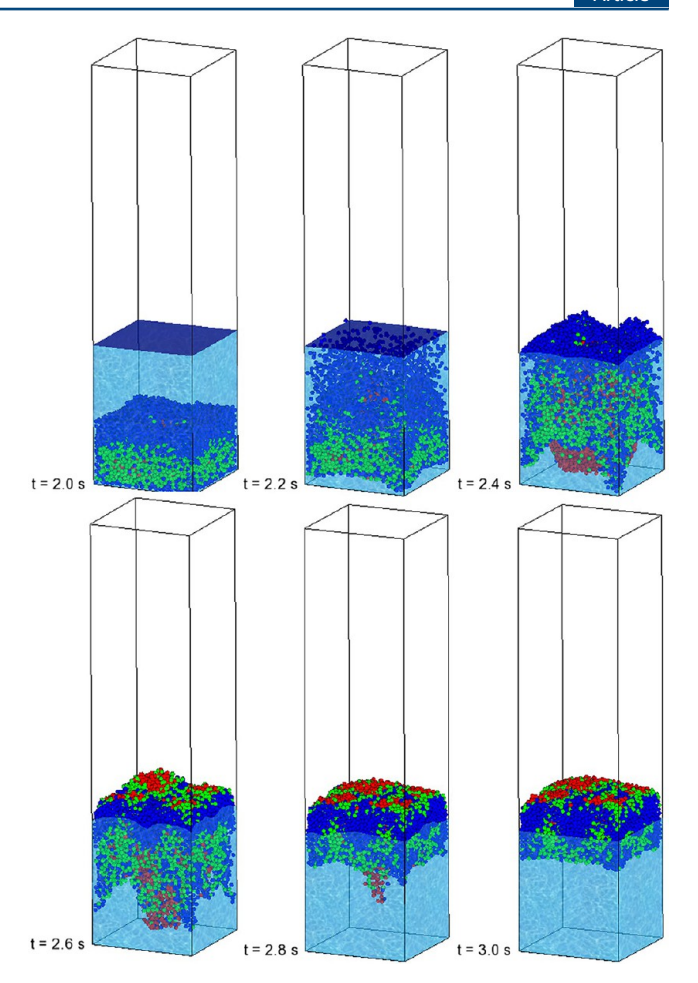
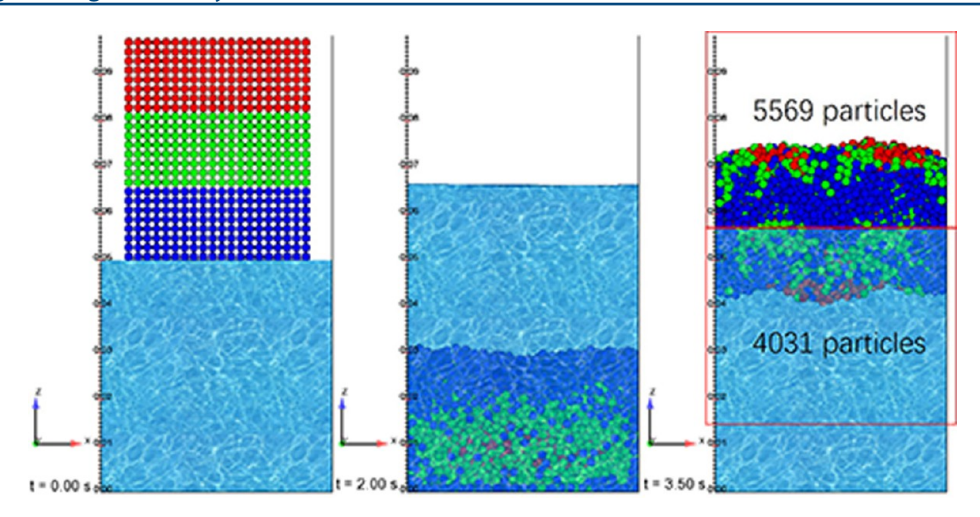


Figure 6. Snapshots of buoyant particles floating out of water.

and the shape of the particle swarm was formed as shown in Figure 6 at different times ( $t=2.4,\ 2.6,\$ and  $2.8\$ s). It can be explained by the interaction between particles, and because the center particles were initially at lower height ( $t=2.0\$ s) the center particles were then squeezed out, like a crowd of people through the theater door. It leads to that particles near the center, not containing particles in four corners, float faster relatively, so the particles in four cornets are slower as shown in Figure 6 at  $t=2.4,\ 2.6,\$ and  $2.8\$ s.

The simulation of particles falling into water and particles floating out of water can be used to check whether the DEM-VOF model has a conservation of volume and high precision, which must be satisfied for the numerical simulation of three phase flow system. In Figure 7, it is obvious that the particles falling into water has caused the distinct rise of the water surface compared with the initial height 0.05 m, and the stable water surface (t = 2.0 s) is near z = 0.06608 m, which can be read from Z-axis scale. The rising of the water surface is theoretically 0.01608 m (=9600  $\times \frac{\pi}{6} (0.002)^3 / (0.05)^2$ ). The simulation results of the particle falling into water indicate that the proposed model in this work has great calculation precision in the volume replacement among three phases. For the floating simulation, the height of stable water surface is about 0.05675 m (t = 3.5 s), and it accounts for about 41.97% ( $=\frac{0.05675 - 0.05}{0.06608 - 0.05}$ ) of the total rise height. Similarly, particles below the water surface (t = 3.5 s) account for about 41.99% (= $\frac{4031}{9600}$ ) of the total particles as seen from t = 3.5 s in Figure 7. The accuracy,



**Figure 7.** Height of water surface at t = 0, 2, and 3.5 s.

robustness, and stability of the model has been validated by the particles falling and floating.

## 4. APPLICATION FOR STIRRED MIXING SYSTEM

Solid-liquid mixing are widely used in the operation of production, transport, and homogenization of various industrial

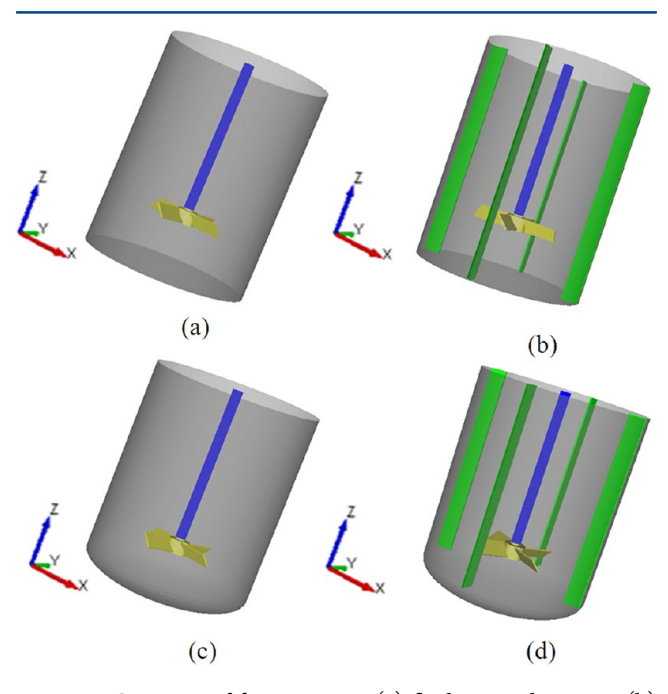


**Figure 8.** Geometry of four agitators: (a) flat-bottomed agitator, (b) flat-bottomed agitator with four baffles, (c) elliptical-head agitator without baffle, (d) elliptical-head agitator with four baffles.

Table 1. Sizes of the Agitators

symbol	meaning	geometric sizes
T	diameter of tank	0.19 m
D	diameter of impeller	T/2
L	height of tank	4T/3
H	level height	T
С	off-bottom height	T/3
E	ellipsoidal head height	T/6
W	blade width and baffle width	D/5

Table 2. Physical Parameter Values of the Fluids and Particles

symbol	meaning	value
$ ho_{ ext{water}}$	water density	1000 kg/m3
$\mu_{ ext{water}}$	water viscosity	0.001 Pa s
$ ho_{ m air}$	air density	1 kg/m3
$\mu_{ m air}$	air viscosity	1e-5 Pa·s
$ ho_{\mathtt{p}}$	particles density	1200 kg/m3
$d_{\rm p}$	particle diameter	2 mm
$N_{ m p}$	number of particles	50000
$arepsilon_{ m p}$	volume fraction of particles	≈ 3.9%
$x_{\rm s}$	mass fraction of solid particles	≈ 4.65%

Table 3. Model Parameter Values in the Solid-Liquid Mixing Simulations

symbol	meaning	value
$Y_{ m wall}$	Young's modulus of wall material	$7 \times 10^{10} \text{ Pa}$
$ u_{\mathrm{wall}}$	Poisson ratio of wall material	0.3
$Y_{p}$	Young's modulus of particle	$1 \times 10^6 \text{ Pa}$
$\nu_{\rm p}$	particle Poisson ratio	0.25
$e_{\mathrm{r}}$	restitution coefficient	0.5
$\mu_{s,ij}$	static friction coefficient	0.5
$\mu_{\mathrm{r},ij}$	rolling friction coefficient	0.01
$\Delta t_{ m DEM}$	DEM time step	$5 \times 10^{-6}$
$\Delta t_{ m CFD}$	CFD time step	$1 \times 10^{-4}$
$\Delta t_C$	coupling time-step	$1 \times 10^{-4}$

processes. As we stated before, previous numerical studies <sup>14–21</sup> about the mixing of stirred solid—liquid all neglected the change of liquid free-surface, so it may be feasible for full baffling stirred tanks in slow stirred speed, equipped with a top-cover lid, or filled with high viscous liquid, wherein the top boundary is taken as a plane below the real liquid surface with little fluctuation, and its type is symmetry boundary. <sup>39</sup> However, the liquid sloshing on free-surface always appears in industrial agitated vessels, like in unbaffled vessels, vessels with single partial baffle, or eccentrically stirred tank, and so on, and this has an important impact on the flow and mixing process. <sup>40–43</sup> The numerical simulations of free-surface flow in unbaffled agitator using the VOF model have been performed by Ciofalo <sup>40</sup> and Haque. <sup>41</sup> Mahmud <sup>42</sup> and Lamarque <sup>43</sup> have performed many numerical analyses to the free-surface flows in magnetic stirrer by adopting VOF model. But they all did not

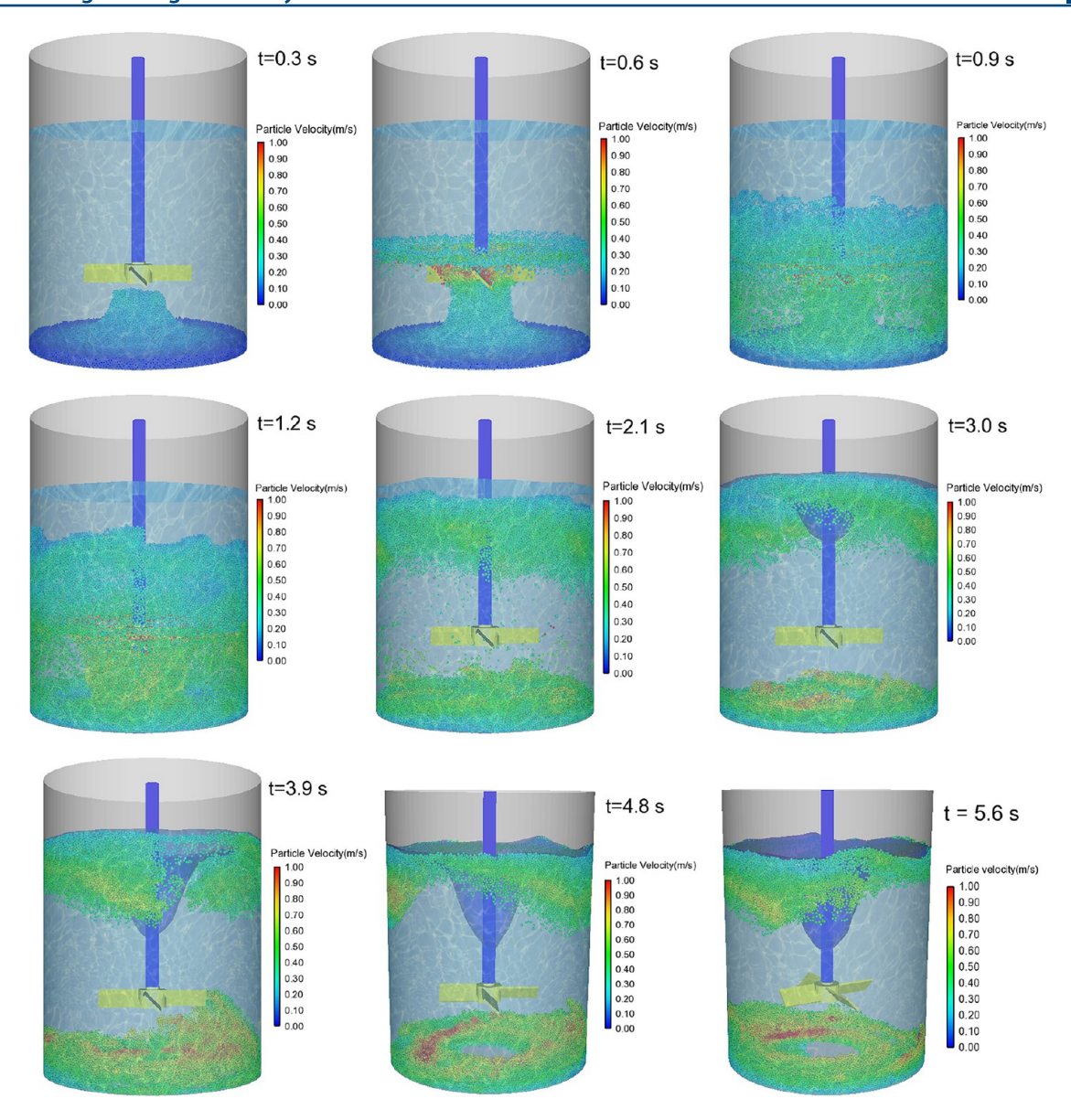


Figure 9. Snapshots of gas-liquid-solid flows in flat-bottomed agitator without baffle.

take into account the effect of suspended particles, even though such vessels are usually used for the operation of suspension, mass transfer, crystallization precipitation, and so on. In this section, the focus is on the application of our proposed DEM—VOF model in free-surface flows with particles in solid—liquid stirred mixing vessels.

In this paper, the free-surface flow with particles in stirred mixing system is computed in four different agitators as illustrated by Figure 8; respectively, they are flat-bottomed agitator without baffles, flat-bottomed agitator with four baffles, elliptical-head agitator with four baffles.

These four geometries have the same diameter T equal to 0.19 m and the same length L equal to 4T/3. The stirred direction is anticlockwise with the down-pumping pitched blade turbine, whose diameter D is equal to T/2. The distance between the impeller center and the vessel bottom is C, which is equal to T/3. Even in the elliptical-head agitator, the distance from the center of the impeller to the apex of the ellipsoidal-head is T/3. The height of the ellipsoidal head is E = T/6 for

the two elliptical-head agitators. The liquid height is equal to the vessel diameter (H=T). The width of the four baffles is T/10 and the blade width is also T/10 (D/5), and their thickness are 0.002 m. All the geometric sizes of the agitators are presented in Table 1.

Table 2 lists the physical parameter values of the fluids and particles studied in this paper. These four geometries have the same mesh scheme, which is that the whole fluid is divided into two zones, respectively their hexahedral mesh size is 6 mm and 4 mm (2–3 times the particle diameter). The parameter values used in the DEM–VOF model are shown in Table 3. In this paper, the effects of the geometric configuration of the stirred tank (the existence of baffles and the shape of bottom) on the particle suspension distribution is studied. As stated above, the four agitators are chosen to perform the simulations under the operating stirred speed ( $N_{\rm p}=400$  RPM) with Reynolds number, Re (=  $\rho NL^2/\mu$ ) of 60196.75. All the simulations were separately carried out on the four computers at the same time, each of which is composed of 8 physical cores, Inter Core(TM) i7-7700K processor with a frequency of 4.2 GHz and 16 Go of

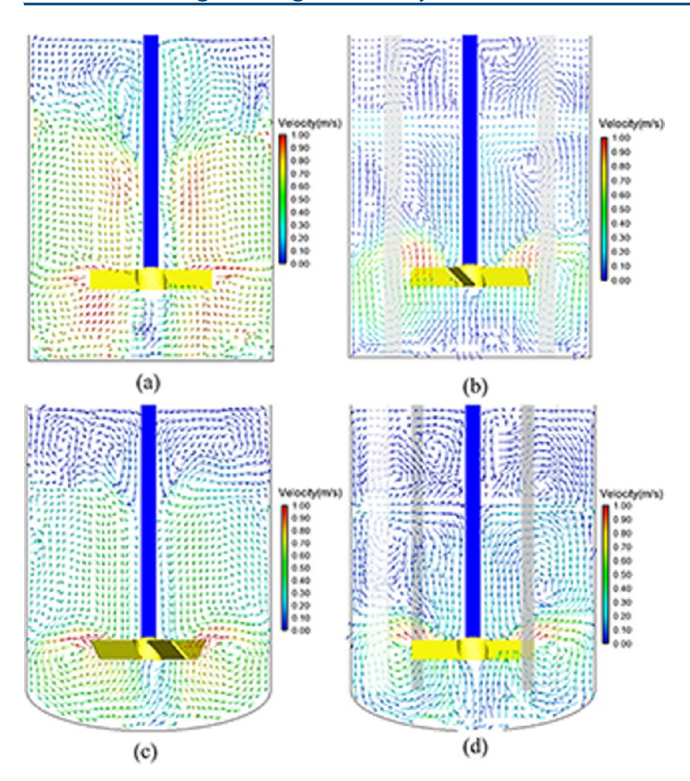


**Figure 10.** Simulated flow patterns in four agitators: (a) flat-bottomed agitator, (b) flat-bottomed agitator with four baffles, (c) elliptical-head agitator without baffle, and (d) elliptical-head agitator with four baffles.

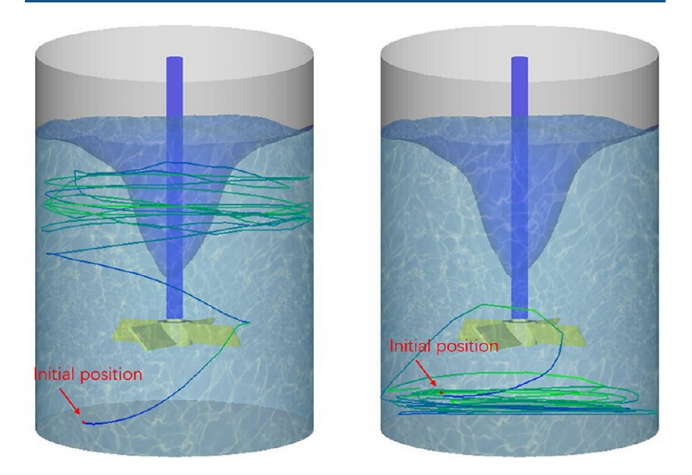


Figure 11. Motion trajectories of two typical particles in flat-bottomed agitator without baffle.

memory, so it can save more time even though each simulation took 20 days.

Figure 9 is the simulation results of the free-surface flows with particles during the startup of the flat-bottomed agitator without baffle. It is obvious that at the beginning (t = 0.3 s) the particles were inhaled at the bottom of the rotating impeller, which is consistent with the calculated results in the literature. Because of the oblique upward agitation of impeller, it leads the oblique upward flow of the surrounding fluid, and the fluid below the impeller is filled accordingly, which flows to the center of the impeller and carries the motion of the particles. The particles moving toward the impeller are then thrown out by the rotation of the impeller (t = 0.6 and 0.9 s). Besides, when the fluid stirred by the impeller is thrown to the wall, it is converted into the vertical two upper and lower velocities. At

the same time, the particles thrown to the wall move upward and downward respectively under the action of fluid (t = 1.2and 2.1 s). Because of the gradual agitation, the swirl motion of the fluid is dominant and the vortex begins to appear (t = 3.0s). Thus, the dominant motion of the particles is swirling motion (t = 3.9 s), and it leads to the central blank area at bottom (t = 4.8 s). Meanwhile, the vortex depth is increasing with the time evolution (t = 3.9 and 4.8 s), and then is almost unchanged in the steady state (t = 5.6 s). Figure 10 shows the calculated flow patterns on a vertical plane of four agitators at quasi steady state (t = 20 s). It is worth recalling that there is no upward flow in the bottom of the impeller at Figure 10a, but conversely it exists in the other agitators (Figure 10b-d). Figure 10a shows that there are upward and downward fluid movements at the impeller height, and it leads to the phenomenon of particles up and down stratification. This can be analyzed from Figure 11, showing the motion trajectory of two typical particles (top and bottom regions) in a flatbottomed agitator without baffle. The baffle can effectively eliminate the swirling flow and transform into vertical flow, so the upward flow in the bottom of impeller is obvious in Figure 10b. Similarly, the upward flow in the bottom of impeller is also obvious in Figure 10c,d because of the elliptical head can concentrate the flow into the bottom center of the container.

Figure 12 is the simulation results of the free-surface flows with particles during the startup of the elliptical-head agitator with baffle. It is obvious that at the beginning  $(t=0.2~\rm s)$  the particles were inhaled at the bottom of the rotating impeller, which is stronger than the calculated results in the flatbottomed agitator without baffle  $(t=0.4~\rm s)$ . It can be seen clearly that the fluid changes into the upward flow after it encounters the baffle, and the particles move upward along the baffle under the fluid action  $(t=0.6~\rm and~0.8~s)$ . Although the baffles can prevent vortex formation, the shape of liquid surface is affected by the motion of particles  $(t=2.0~\rm and~3.0~s)$ .

Figure 13 is the simulation result of water surface and particle dispersion on quasi-steady state ( $t=20.0~\rm s$ ) in four types agitators. It is found that Figure 13a has the deepest vortex, followed by Figure 13c, and the water surface in Figure 13b has only a depression in the central region. Obviously, the water surface fluctuation in Figure 13d is the smallest. This leads to a conclusion that the elliptical head weakens the swirling flow to some extent. Besides, it is found that there are dead zones that particles deposit behind the baffle in Figure 13b. In order to better observe the dispersion of particles, the half of visualization in four agitators was Figure 14. In Figure 14b,d, some particles unceasingly move upward to form a conical (or umbrella) area. There is the central blank area at bottom in Figure 14a,c, but there are particles are moving upward near the central blank area in Figure 14c.

In order to further quantify the dispersion of particles in four different solid—liquid stirrers, the relative standard deviation (RSD) of the number of particles in the sample volume is defined in this paper, which is derived from Jovanović<sup>44</sup> and defined as

RSD = 
$$\frac{\sigma}{N_{\text{av}}}$$
,  $\sigma = \sqrt{\frac{\sum_{i=1}^{M} (N_i - N_{\text{av}})^2}{M - 1}}$ . (19)

where M is the sample numbers,  $N_i$  is the particle numbers in sample volume i, and  $N_{\rm av}$  is the average particle numbers of all volumes. It is obvious that the smaller the RSD value indicates the better the dispersion of the particles. In this work, 27 (M =

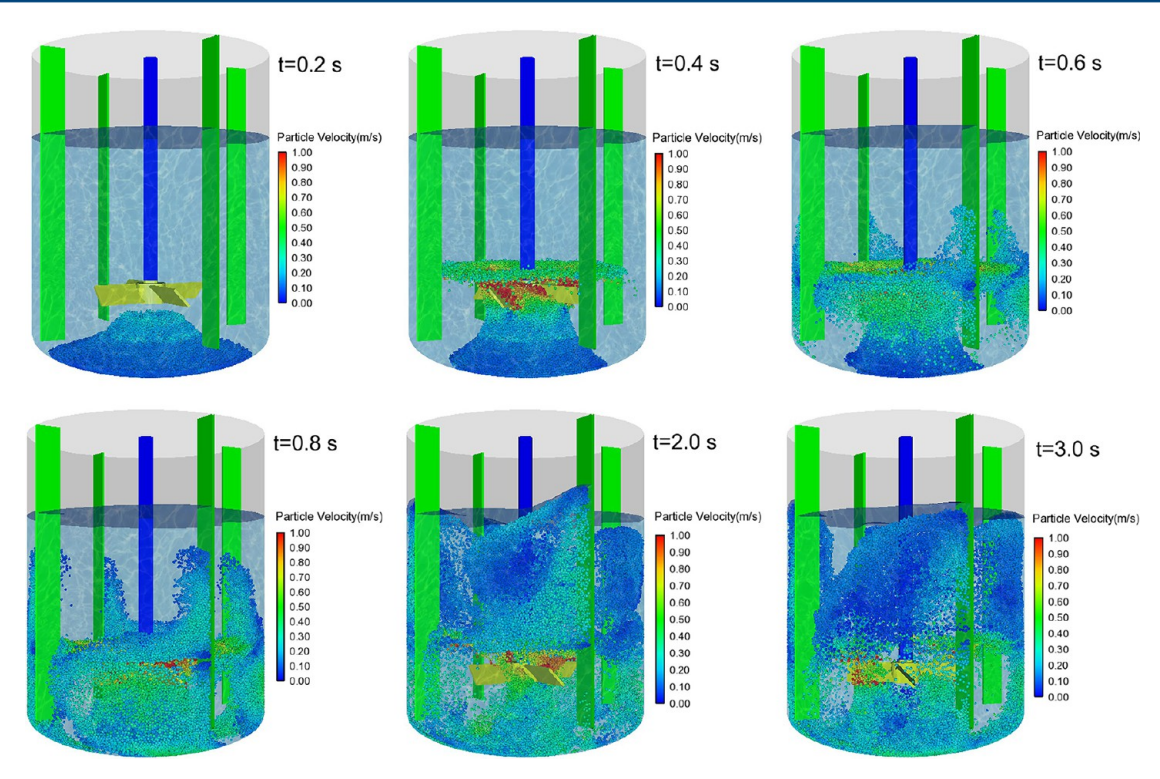
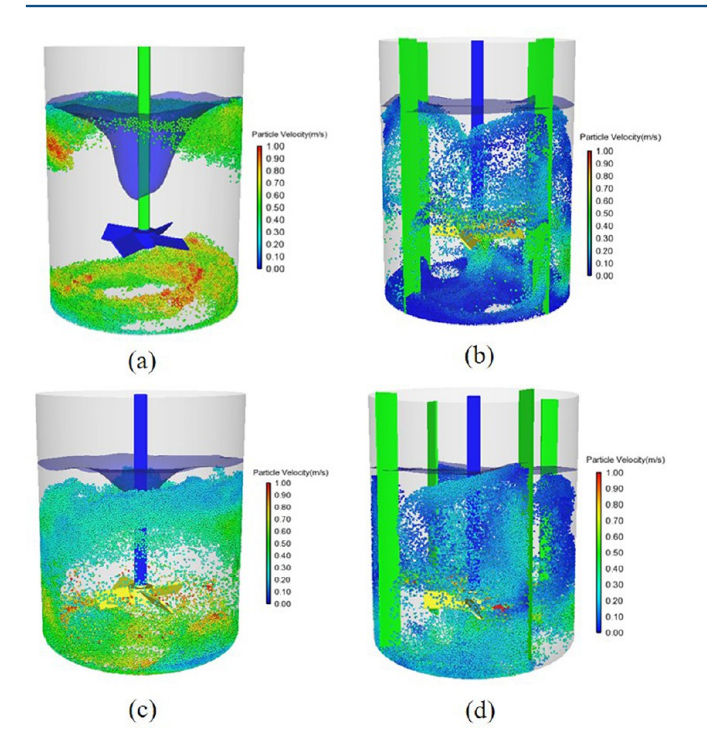


Figure 12. Snapshots of gas-liquid-solid flows in elliptical-head agitator with baffle.



**Figure 13.** Water surface and particle dispersion on quasi-steady state (t = 20.0 s), (a) flat-bottomed agitator, (b) flat-bottomed agitator with four baffles, (c) elliptical-head agitator without baffle, and (d) elliptical-head agitator with four baffles.

27) equal volume regions are adopted and the RSD with time evolution on four agitators is plotted in Figure 15. As shown, the RSD in four agitators are all decreasing during the start-up. But the RSD in flat-bottomed agitator without baffle encounter an increase due to the phenomenon of particles up and down stratification mentioned above. Then the all RSD fluctuates in a

small range except the flat-bottomed agitator with baffles, that is, because there are amounts of resident particles in dead zones and the morphology of suspended particles is sometimes sparse, sometimes dense. They can be seen from the offered videos in the Supporting Information. The time evolution of four agitators imply that the elliptical-head agitator with baffle has the best dispersion performance of particles, which agrees well to the related content of the book *Handbook of Industrial Mixing*. <sup>13</sup>

#### 5. CONCLUSIONS

In this study, we extend the DEM-VOF model to simulate the turbulent flow by means of Reynolds turbulence model, especially for modeling free-surface flows with particles in solid-liquid mixing. The VOF method and the DEM method are used to calculate the fluid free-surface and the particles motion, respectively. Besides, a novel virtual dual-grid porosity model is employed to describe interphase volume replacements between fluids and particles, which can overtake the calculation instabilities when mesh size  $\Delta x < 3d_p$ . Then, the proposed model is validated by using two kinds of tests: single particle sedimentation and the interaction between water surface and particle swarm, which includes the falling of sinking particles and the floating of buoyant particles. The simulation results of particle sedimentation tests indicate that the particle-fluids interaction force can be correctly calculated and coupled by the proposed DEM-VOF model. The accuracy in volume conservation between three-phases has been validated and produced by the simulation of falling of sinking particles and floating of the buoyant particles. The complex deformation of water surface and the motion of particles are also consistent to literatures. Then, the performance of particle dispersion in four different configuration agitators has been simulated by our proposed model, and it is first reported that the DEM-VOF model is involved to the free-surface flows with particles in

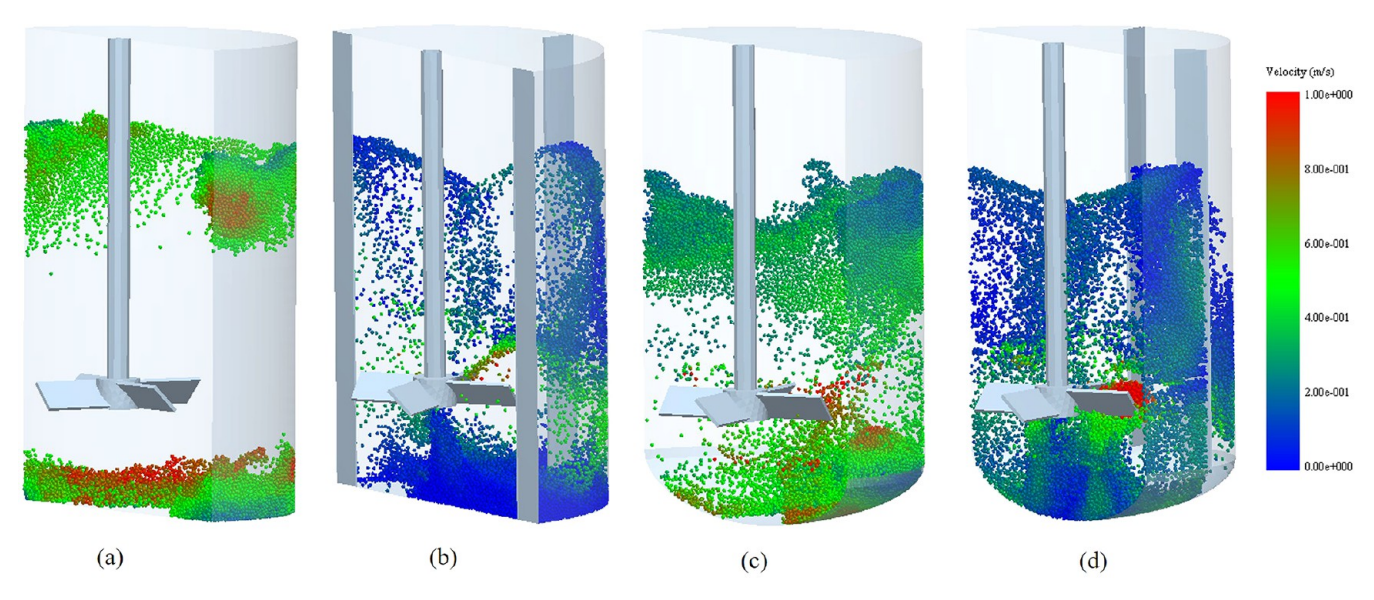


**Figure 14.** Half of visualization in four agitators on quasi-steady state (t = 20.0 s), (a) flat-bottomed agitator, (b) flat-bottomed agitator with four baffles, (c) elliptical-head agitator without baffle, and (d) elliptical-head agitator with four baffles.

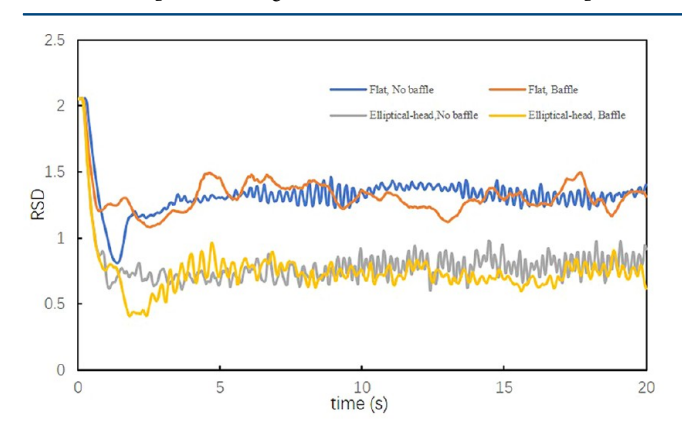


Figure 15. Time evolution of RSD in four agitators.

solid—liquid stirred tank. In order to facilitate readers to understand the flow visually, the videos of each dynamic simulation have been attached in the Supporting Information. In the future work, the DEM—VOF model will be further used to understand and analyze more complex free-surface flows with particles, especially for the mixing of floating particles, whose research is mainly based on experimental measurements and numerical simulation of fluid mechanics is relatively scarce.

## ASSOCIATED CONTENT

#### Supporting Information

The Supporting Information is available free of charge on the ACS Publications website at DOI: 10.1021/acs.iecr.7b04833.

The falling of sinking particles and the floating of buoyant particles (AVI)

The stirring process in the four different agitators, Flat-NoBaffle (AVI)

The stirring process in the four different agitators, Flat-Baffle (AVI)

The stirring process in the four different agitators, Elliptical-NoBaffle (AVI)

The stirring process in the four different agitators, Elliptical-Baffle (AVI)

Table S1 to S2 (PDF)

### AUTHOR INFORMATION

#### Corresponding Author

\*E-mail: wjingtao928@tju.edu.cn.

ORCID ®

Jingtao Wang: 0000-0002-1712-7898

**Notes** 

The authors declare no competing financial interest.

## ACKNOWLEDGMENTS

Supported by National Natural Science Foundation of China (21376162 and 21576185).

## REFERENCES

- (1) Pozzetti, G.; Peters, B. A. Multiscale DEM-VOF method for the simulation of three-phase flows. *Int. J. Multiphase Flow* **2018**, *99*, 186.
- (2) Huang, Q.; Yang, C.; Yu, G.; Mao, Z. S. CFD simulation of hydrodynamics and mass transfer in an internal airlift loop reactor using a steady two-fluid model. *Chem. Eng. Sci.* **2010**, *65*, 5527–5536.
- (3) Qiu, L. C. Numerical modeling of liquid-particle flows by combining SPH and DEM. *Ind. Eng. Chem. Res.* **2013**, *52*, 11313–11318.
- (4) Zhu, H. P.; Zhou, Z. Y.; Yang, R. Y.; Yu, A. B. Discrete particle simulation of particulate systems: theoretical developments. *Chem. Eng. Sci.* **2007**, *62*, 3378–3396.
- (5) Zhu, H. P.; Zhou, Z. Y.; Yang, R. Y.; Yu, A. B. Discrete particle simulation of particulate systems: a review of major applications and findings. *Chem. Eng. Sci.* **2008**, *63*, 5728–5770.
- (6) Patankar, N. A.; Singh, P.; Joseph, D. D.; Glowinski, R.; Pan, T. W. A new formulation of the distributed Lagrange multiplier/fictitious domain method for particulate flows. *Int. J. Multiphase Flow* **2000**, *26*, 1509–1524.
- (7) Goniva, C.; Gruber, K.; Kloss, C. Sediment erosion a numerical and experimental study. *River Flow.* **2012**, 415.
- (8) Gruber, K. Sediment transport in open channel flows experimental investigation and numerical simulation of local scour development downstream of a weir. Ph.D. Thesis, Johannes Kepler University, Linz, Austria, 2012.
- (9) Jing, L.; Kwok, C. Y.; Leung, Y. F.; Sobral, Y. D. Extended CFD-DEM for free-surface flow with multi-size granules. *Int. J. Numer. Anal. Methods Geomech.* **2016**, *40*, 62–79.

- (10) Chen, Y.; Yu, C.; Liu, M.; Chen, S.; Chen, Y. Particle dispersion in a partially filled rotating cylindrical tank. *Chem. Eng. Res. Des.* **2016**, *111*, 1–12.
- (11) Sun, X.; Sakai, M. Three-dimensional simulation of gas—solid—liquid flows using the DEM—VOF method. *Chem. Eng. Sci.* **2015**, *134*, 531–548.
- (12) Guo, L.; Morita, K. Numerical simulation of 3D sloshing in a liquid—solid mixture using particle methods. *Int. J. Numer. Meth. Eng.* **2013**, 95, 771–790.
- (13) Handbook of Industrial Mixing science and practice; Paul, E. L., Atiemo-Obeng, V. A., Kresta, S. M., Eds.; John Wiley & Sons, 2004.
- (14) Tamburini, A.; Cipollina, A.; Micale, G.; Ciofalo, M.; Brucato, A. Dense solid—liquid off-bottom suspension dynamics: simulation and experiment. *Chem. Eng. Res. Des.* **2009**, *87*, 587—597.
- (15) Tamburini, A.; Cipollina, A.; Micale, G.; Brucato, A.; Ciofalo, M. CFD simulations of dense solid—liquid suspensions in baffled stirred tanks: Prediction of the minimum impeller speed for complete suspension. *Chem. Eng. J.* **2012**, *193-194*, 234–255.
- (16) Derksen, J. J. Numerical simulation of solids suspension in a stirred tank. *AIChE J.* **2003**, *49*, 2700–2714.
- (17) Derksen, J. J. Highly resolved simulations of solids suspension in a small mixing tank. *AIChE J.* **2012**, *58*, 3266–3278.
- (18) Shao, T.; Hu, Y.; Wang, W.; Jin, Y.; Cheng, Y. Simulation of solid suspension in a stirred tank using CFD-DEM coupled approach. *Chin. J. Chem. Eng.* **2013**, *21*, 1069–1081.
- (19) Blais, B.; Lassaigne, M.; Goniva, C.; Fradette, L.; Bertrand, F. Development of an unresolved CFD–DEM model for the flow of viscous suspensions and its application to solid–liquid mixing. *J. Comput. Phys.* **2016**, 318, 201–221.
- (20) Blais, B.; Bertrand, F. CFD-DEM investigation of viscous solid—liquid mixing: Impact of particle properties and mixer characteristics. *Chem. Eng. Res. Des.* **2017**, *118*, 270–285.
- (21) Blais, B.; Bertrand, O.; Fradette, L.; Bertrand, F. CFD-DEM simulations of early turbulent solid-liquid mixing: Prediction of suspension curve and just-suspended speed. *Chem. Eng. Res. Des.* **2017**, *123*, 388.
- (22) Link, J. M.; Cuypers, L. A.; Deen, N. G.; Kuipers, J. A. M. Flow regimes in a spout—fluid bed: A combined experimental and simulation study. *Chem. Eng. Sci.* **2005**, *60*, 3425–3442.
- (23) Tsuji, Y.; Tanaka, T.; Ishida, T. Lagrangian numerical simulation of plug flow of cohesionless particles in a horizontal pipe. *Powder Technol.* **1992**, *71*, 239–250.
- (24) Johnson, K. L.; Johnson, K. Normal contact of elastic solids: Hertz theory. *Contact mechanics* **1985**, 84–106.
- (25) Hertz, H. Über die Berührung fester elastischer Körper. J. Reine. Angew. Math. 1882, 92, 156–171.
- (26) Mindlin, R. D. Elastic spheres in contact under varying oblique forces. *Trans. ASME, J. Appl. Mech.* **1953**, *20*, 327–344.
- (27) Mindlin, R. D. Compliance of elastic bodies in contact. *J. Appl. Mech.* 1949, 16, 259–268.
- (28) ANSYS FLUENT Theory Guide Inc., release 15; ANSYS Academic Research, 2013.
- (29) Anderson, T. B.; Jackson, R. Fluid mechanical description of fluidized beds. Equations of motion. *Ind. Eng. Chem. Fundam.* **1967**, *6*, 527–539.
- (30) Gibson, M. M.; Launder, B. E. Ground effects on pressure fluctuations in the atmospheric boundary layer. *J. Fluid Mech.* **1978**, *86*, 491–511.
- (31) Launder, B. E. Second-moment closure: present... and future? *Int. J. Heat Fluid Flow* **1989**, *10*, 282–300.
- (32) Launder, B. E.; Reece, G. J.; Rodi, W. Progress in the development of a Reynolds-stress turbulence closure. *J. Fluid Mech.* **1975**, *68*, 537–566.
- (33) Brackbill, J. U.; Kothe, D. B.; Zemach, C. A continuum method for modeling surface tension. *J. Comput. Phys.* **1992**, *100*, 335–354.
- (34) Zhao, J.; Shan, T. Coupled CFD–DEM simulation of fluid–particle interaction in geomechanics. *Powder Technol.* **2013**, 239, 248–258.

- (35) Kloss, C.; Goniva, C.; Hager, A.; Amberger, S.; Pirker, S. Models, algorithms and validation for opensource DEM and CFD-DEM. *Prog. Comput. Fluid Dyn.* **2012**, *12*, 140–52.
- (36) Kawaguchi, T.; Sakamoto, M.; Tanaka, T.; Tsuji, Y. Quasi-three-dimensional numerical simulation of spouted beds in cylinder. *Powder Technol.* **2000**, *109*, 3–12.
- (37) Pirker, S.; Kahrimanovic, D.; Goniva, C. Improving the applicability of discrete phase simulations by smoothening their exchange fields. *Appl. Math. Model.* **2011**, *35*, 2479–2488.
- (38) Robinson, M.; Ramaioli, M.; Luding, S. Fluid—particle flow simulations using two-way-coupled mesoscale SPH—DEM and validation. *Int. J. Multiphase Flow* **2014**, *59*, 121–134.
- (39) Ali, B. A.; Janiga, G.; Temmel, E.; Seidel-Morgenstern, A.; Thévenin, D. Numerical analysis of hydrodynamics and crystal motion in a batch crystallizer. *J. Cryst. Growth* **2013**, *372*, 219–229.
- (40) Ciofalo, M.; Brucato, A.; Grisafi, F.; Torraca, N. Turbulent flow in closed and free-surface unbaffled tanks stirred by radial impellers. *Chem. Eng. Sci.* **1996**, *51*, 3557–3573.
- (41) Haque, J. N.; Mahmud, T.; Roberts, K. J.; Rhodes, D. Modeling turbulent flows with free-surface in unbaffled agitated vessels. *Ind. Eng. Chem. Res.* **2006**, *45*, 2881–2891.
- (42) Mahmud, T.; Haque, J. N.; Roberts, K. J.; Rhodes, D.; Wilkinson, D. Measurements and modelling of free-surface turbulent flows induced by a magnetic stirrer in an unbaffled stirred tank reactor. *Chem. Eng. Sci.* **2009**, *64*, 4197–4209.
- (43) Lamarque, N.; Zoppé, B.; Lebaigue, O.; Dolias, Y.; Bertrand, M.; Ducros, F. Large-eddy simulation of the turbulent free-surface flow in an unbaffled stirred tank reactor. *Chem. Eng. Sci.* **2010**, *65*, 4307–4322.
- (44) Jovanović, A.; Pezo, M.; Pezo, L.; Lević, L. DEM/CFD analysis of granular flow in static mixers. *Powder Technol.* **2014**, 266, 240–248.